Article

Enhanced Adsorption Capacities of Fungicides Using Peanut Shell Biochar via Successive Chemical Modification with KMnO$_4$ and KOH

Yong-Gu Lee [1], Jaegwan Shin [2], Jinwoo Kwak [2], Sangwon Kim [2], Changgil Son [2], Geon-Youb Kim [3], Chang-Ha Lee [3] and Kangmin Chon [1,2,*]

[1] Department of Environmental Engineering, College of Engineering, Kangwon National University, 1 Kangwondaehak-gil, Chuncheon-si 24341, Korea; yglee19@kangwon.ac.kr
[2] Department of Integrated Energy and Infra System, Kangwon National University, 1 Kangwondaehak-gil, Chuncheon-si 24341, Korea; jgshin13@kangwon.ac.kr (J.S.); kh01kjw@kangwon.ac.kr (J.K.); swkim9521@kangwon.ac.kr (S.K.); numer5@kangwon.ac.kr (C.S.)
[3] Corporate Collaboration Center, Sungkyunkwan University, 2066, Seobu-ro, Jangan-gu, Suwon-si 16419, Korea; gykim@purivid.com (G.-Y.K.); ha1991@purivid.com (C.-H.L.)
[*] Correspondence: kmchon@kangwon.ac.kr; Tel.: +82-33-250-6352

Abstract: This study explored the effects of peanut shell biochar (PSB) on the adsorption capacities of fungicides with and without successive chemical modifications, using KMnO$_4$ and KOH (PSB$_{OX-A}$), in order to provide a valuable understanding of their adsorption mechanisms and behaviors. To this end, the physicochemical properties of PSB and PSB$_{OX-A}$ were examined by using the Brunauer–Emmett–Teller method, Fourier transform infrared spectroscopy, and scanning electron microscopy with an energy dispersive X-ray spectrometer. The effects of temperature, ionic strength, and humic acids on the adsorption of fungicides, using PSB and PSB$_{OX-A}$, were estimated through batch experiments. Furthermore, adsorption kinetics, isotherms, and thermodynamics were studied. The maximum adsorption capacities of fungicides by PSB$_{OX-A}$ were estimated to be more notable (Q_{max} of carbendazim = 531.2 μmol g^{-1}, Q_{max} of pyrimethanil = 467.7 μmol g^{-1}, and Q_{max} of tebuconazole = 495.1 μmol g^{-1}) than PSB (Q_{max} of carbendazim = 92.6 μmol g^{-1}, Q_{max} of pyrimethanil = 61.7 μmol g^{-1}, and Q_{max} of tebuconazole = 66.7 μmol g^{-1}). These findings suggest that successive chemical modification using KMnO$_4$ and KOH could potentially be used to effectively fabricate PSB to remove fungicides in water-treatment processes.

Keywords: adsorption; biochar; fungicides; oxidative and alkali modification; peanut shell

1. Introduction

Fungicides are chemicals that are used to prevent fungal infections in seeds and plants. Rapid growth in the global population has led to a rise in the demand for crop yields, which has subsequently increased the use of fungicides [1]. This increase can act as a non-point source of pollution in surface water via runoff [2]. Carbendazim (CAR; methyl *N*-(1H-benzimidazol-2-yl)carbamate), pyrimethanil (PYR; 4,6-dimethyl-*N*-phenylpyrimidin-2-amine), and tebuconazole (TEB; 1-(4-chlorophenyl)-4,4-dimethyl-3-(1,2,4-triazol-1-ylmethyl)pentan-3-ol) have been frequently detected in surface waters (CAR = 0.6–6 μg L^{-1}, PYR = 4 ng L^{-1}, and TEB = 0.6–200 μg L^{-1}) [3–5]. Even though the aforementioned fungicides are generally regarded as having low toxicity, their high chemical stability and slow degradability pose potential risks to aquatic organisms and human health [1]. However, few studies have focused on developing efficient treatments to remove fungicide pollution from water resources [6].

Recently, several researchers have recognized that adsorption is the most efficient treatment option; moreover, its operating cost for fungicide removal in water-treatment plants is low [6]. Activated carbon (AC), a representative adsorbent, is commonly utilized

in the water-treatment process because it has a large specific surface area, porous structure, and a wide range of pH reactivity [7]. Moreover, various nanomaterials, including graphene and metal nanoparticles [8] and carbon nanotubes [9], have been used to remove fungicides from water. Zhaokun et al. demonstrated the efficient removal of triazole fungicides on graphene using metal nanoparticles [8]. Chen et al. fabricated magnetic carbon nanotubes for the adsorption of fungicides [9]. Although nanomaterials are beneficial due to their high efficiency and fast adsorption, their physicochemical properties (e.g., small size, persistence, and non-biodegradation) can be detrimental to humans and the environment. Furthermore, the uses of AC and nanomaterials in real-scale water-treatment processes are limited because of their high production and operation costs [10].

In recent years, new developments in waste-reuse technology, such as biochar derived from agricultural and food residues, including peanut shells and ground coffee waste, have become a global focus for research [11,12]. Furthermore, biochar can be a great alternative to AC because of its high specific surface area, porous structure, and various surface functional groups [13]. The adsorption capacity of biochar may be influenced by biomass, carbonization conditions (temperature and retention time), and chemical modification [14]. Chemical modification methods involving oxidative and alkali agents may improve the surface functionality of biochar and enhance electrostatic repulsive interactions with organic pollutants in water [15]. Peanut is a common agricultural residue in the United States. Considerable quantities (about 30 thousand metric tons) of peanuts shell are used to feed and energy resources each year [16]. The main components of peanut shells have been reported to be fiber (60–70 wt.%), cellulose (34–45 wt.%), and lignin (27–33 wt.%). The peanut shells have a cellulose–lignin layer that considerably affects the porous structure and the pyrolysis behavior [17]. In order to make peanut shells an eco-friendly and low-cost alternative adsorbent, they need to be converted into valuable resources. However, most studies have explored the adsorption mechanism by using peanut shell biochar (PSB) of heavy metals, such as Ni(II), Cd(II), Cu(II), Pb(II), and Zn(II) [16,18]. Moreover, there is a need for a comprehensive study on the effects of successive chemical modification of PSB with potassium permanganate ($KMnO_4$) and potassium hydroxide (KOH) on the adsorption behavior of fungicides.

This study investigated the adsorption behaviors of fungicides by PSB and successive $KMnO_4$ and KOH modified PSB (PSB_{OX-A}) to compare the physicochemical properties of PSB and PSB_{OX-A} (surface morphology, porous structure, bulk elemental composition, and surface functional groups). The adsorption behavior of fungicides (i.e., CAR, PYR, and TEB) by PSB and PSB_{OX-A} was optimized and evaluated through batch experiments. The adsorption kinetics, isotherms, and thermodynamics were used to identify the primary adsorption mechanisms of CAR, PYR, and TEB, using PSB and PSB_{OX-A}. Furthermore, the effects of temperature, ionic strength, and humic acids (HA) on the adsorption of CAR, PYR, and TEB by PSB and PSB_{OX-A} were examined.
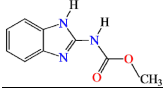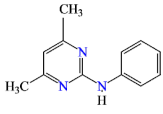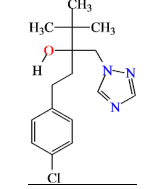
2. Materials and Methods

2.1. Chemicals

All chemicals and fungicides were of analytical grade. CAR (methyl *N*-(1H-benzimidazol-2-yl)carbamate), PYR (4,6-dimethyl-*N*-phenylpyrimidin-2-amine), TEB (1-(4-chlorophenyl)-4,4-dimethyl-3-(1,2,4-triazol-1-ylmethyl)pentan-3-ol), $KMnO_4$, KOH, sodium hydroxide (NaOH), hydrochloric acid (HCl), sodium chloride (NaCl), and HA were purchased from Sigma-Aldrich (St. Louis, MO, USA). High-performance liquid chromatography (HPLC)-grade acetonitrile (ACN) was obtained from J.T. Baker (Deventer, Netherlands), and phosphoric acid (H_3PO_4) was purchased from FUJIFILM Wako Pure Chemical Corporation (Osaka, Japan). The use of ACN is due to its strong solvation properties for a wide range of polar and nonpolar organic solutes and advantageous properties, including low viscosity and low toxicity [19]. A mixed stock solution containing CAR, PYR, and TEB (concentration of each fungicide = 1 mmol L^{-1}) was prepared by using ACN and deionized (DI) water (50:50, *v/v*). DI water was produced by using a Nanopure Water System (electrical

resistivity >18.2 MΩ cm^{-1}; Barnstead, Lake Balboa, CA, USA), and it was used to make the samples. These stock solutions were stored at 4 °C, in the dark, prior to use. The physicochemical properties of CAR, PYR, and TEB are summarized in Table 1.

Table 1. Physicochemical properties of the selected fungicides.

| Compounds (Abbreviation) | Formula | Structure | Molecular Weight (g mol^{-1}) | Charge [a] | | | Log D [a] | | | pK_a [a] | Solubility in Water [b] (g L^{-1}, pH 7) |
				pH 3.0	pH 7.0	pH 11.0	pH 3.0	pH 7.0	pH 11.0		
Carbendazim (CAR)	C$_9$H$_9$N$_3$O$_2$		191.19	1	0	−1	0.73	1.80	1.01	4.28	0.008
Pyrimethanil (PYR)	C$_{12}$H$_{13}$N$_3$		199.25	1	0	0	1.87	2.43	2.43	3.44	0.121
Tebuconazole (TEB)	C$_{16}$H$_{22}$ClN$_3$O		307.82	0	0	0	3.65	3.69	3.69	2.01	0.036

[a] ChemAxon (http://www.chemicalize.org, 2 January 2021). [b] Hazardous Substances Data Bank (http://pubchem.ncbi.nih.gov, 2 January 2021).

2.2. Preparation of PSB and PSB$_{OX-A}$

The detailed preparation method of the PSB via successive chemical modification with KMnO$_4$ and KOH was modified in a previous study [20].

2.2.1. PSB

Peanut shells were purchased from a local grocery store in Chuncheon-si (Gangwon-do, Korea). They were rinsed several times with DI water and dried in an oven for 24 h, at 105 °C. The PSB was pyrolyzed by using a tubular furnace (PyroTech, Namyangju-si, Korea) for 2 h, at 700 °C, under N$_2$ atmosphere (heating rate = 10 °C min^{-1}; the N$_2$ flow rate = 0.25 L min^{-1}). After the entire procedure was completed, the produced PSB was rinsed with DI water and dried in an oven at 105 °C, for 12 h.

2.2.2. PSB$_{OX-A}$

To enhance the surface functionality of PSB, the PSB (5 g) produced was mixed with 0.5% KMnO$_4$ (10 mL) by stirring at 20 ± 0.5 °C for 4 h and drying in an oven, at 60 °C, for 4 h. The modified PSB with KMnO$_4$ was pyrolyzed by using a tubular furnace at 700 °C, for 2 h, under N$_2$ atmosphere (heating rate = 10 °C min^{-1}; N$_2$ flow rate = 0.25 L min^{-1}). The modified PSB with KMnO$_4$ was rinsed with DI water several times and dried in an oven, at 105 °C, for 12 h. Furthermore, the modified PSB with KMnO$_4$ was added to KOH (15 g) and pyrolyzed in a tubular furnace, at 700 °C (heating rate = 10 °C min^{-1}), for 1 h, under N$_2$ atmosphere (flow rate = 0.25 L min^{-1}). The PSB$_{OX-A}$ produced was rinsed with DI water several times and dried in an oven, at 60 °C, for 24 h. The dried PSB$_{OX-A}$ was passed through a 100-mesh sieve, to maintain a uniform size, after which it was stored in a desiccator prior to analysis.

2.3. Characteristics of PSB and PSB$_{OX-A}$
2.3.1. Specific Surface Area and Porosity

The specific surface areas (m^2 g^{-1}) of PSB and PSB$_{OX-A}$ were determined by using the Brunauer–Emmett–Teller (BET) method on the N$_2$ adsorption–desorption isotherms

at 77.3 K in the relative pressure range of 0.01–0.99 (ASAP 2020 Plus, Micromeritics, GA, USA). The total pore volume ($cm^3 g^{-1}$) and average pore size (nm) were calculated by using the Barrett–Joyner–Halenda (BJH) method [21].

2.3.2. Elemental Compositions

The elemental compositions (i.e., carbon (C), hydrogen (H), oxygen (O), nitrogen (N), and sulfur (S)) of PSB and PSB_{OX-A} were measured by using a EuroEA3000 elemental analyzer (EuroVector S.p.A, Via F.lli Cuzio, Italy). Ash content was calculated by subtracting the C, H, O, N, and S contents from the total amount of PSB and PSB_{OX-A}. The atomic molar ratios of H/C and O/C + N/C were used to reveal the aromaticity and polarity of PSB and PSB_{OX-A}, respectively [21].

2.3.3. Scanning Electron Microscopy Analysis

The surface morphologies of PSB and PSB_{OX-A} were identified by using an S-4800 scanning electron microscope (SEM; Hitachi, Tokyo, Japan) with an energy dispersive X-ray (EDX) spectrometer.

2.3.4. Fourier Transform Infrared Spectroscopy Analysis

Fourier transform infrared (FTIR) spectroscopy with a KBr pellet was used to qualitatively analyze the surface functional groups of PSB and PSB_{OX-A} ranging between 400 and 4000 cm^{-1} (Vertex 70, Bruker, Billerica, MA, USA).

2.4. Analytical Methods

The concentrations of CAR, PYR, and TEB in the samples were measured by using HPLC coupled with a column (XDB C18; ZORBAX Eclipse®, 4.6 mm × 150 mm, inner diameter = 5 µm; Agilent, Santa Clara, CA, USA) and a UVA detector (SPD-10AVP, Shimadzu, Kyoto, Japan) at 210 nm. The mobile phase (CAN: 0.05 M H_3PO_4 (50:50, *v*/*v*)) was operated under isocratic conditions (flow rate = 1.0 mL min^{-1}) for 15 min. Various sample conditions were used to evaluate the effects of temperature, ionic strength, and HA on the adsorption of CAR, PYR, and TEB when using PSB and PSB_{OX-A} (the concentration of each fungicide = 10 µmol L^{-1}, temperature = 15–35 °C, concentrations of NaCl = 0–0.1 M, and concentration of HA = 5 mg L^{-1}). All adsorption experiments were conducted in triplicate, using a shaking incubator (Vision Scientific, Daejeon, Korea). Then, the sample solutions were filtered by using a nominal pore size of 0.7 µm glass fiber filter (GF/F; Whatman, Maidstone, UK) to eliminate PSB and PSB_{OX-A}.

The amounts of CAR, PYR, and TEB adsorbed per unit mass of PSB and PSB_{OX-A} at equilibrium, Q_e (µmol g^{-1}), and removal efficiencies (%) of CAR, PYR, and TEM by PSB and PSB_{OX-A} were calculated by using the following equations:

$$Q_e = \frac{(C_0 - C_e)V}{M}, \tag{1}$$

$$Removal\ efficiency\ of\ fungicide\ (\%) = \frac{C_0 - C_e}{C_0} \times 100, \tag{2}$$

where C_0 and C_e (µmol L^{-1}) are the initial and equilibrium concentrations of CAR, PYR, and TEB, respectively. V (L) is the sample solution volume, and M (g) is the amount of PSB and PSB_{OX-A}.

The adsorption kinetics of CAR, PYR, and TEB were examined by using the pseudo-first-order (Equation (3)) and pseudo-second-order (Equation (4)) kinetic models (adsorbent dosage = 50 mg L^{-1}, initial concentration of each fungicide = 10 µmol L^{-1}, contact time = 0–24 h, agitation speed = 150 rpm, temperature = 25 °C, and pH = 7.0) [22]:

$$Q_t = Q_e(1 - \frac{1}{\exp(k_1 t)}, \tag{3}$$

$$Q_t = Q_e \left(1 - \frac{1}{1 + Q_e k_2 t} \right), \tag{4}$$

where Q_t (μmol g^{-1}) is the amount of adsorbed CAR, PYR, and TEB on PSB and PSB$_{OX-A}$ at adsorption time t (h). Moreover, k_1 (1/h) and k_2 (g μmol^{-1}·h) are the rate constants of the pseudo-first-order and pseudo-second-order models, respectively.

The adsorption isotherms of CAR, PYR, and TEB were investigated at five different initial concentrations (10, 20, 30, 40, and 50 μmol L^{-1}), under fixed conditions (adsorbent dosage = 50 mg L^{-1}, contact time = 24 h, agitation speed = 150 rpm, temperature = 25 °C, and pH = 7.0) [23].

$$\text{Langmuir Isotherm}: \ Q_e = \frac{Q_{max} K_L C_e}{1 + K_L C_e}, \tag{5}$$

$$\text{Freundlich isotherm}: \ Q_e = K_F C_e^{1/n}, \tag{6}$$

where Q_{max} (μmol g^{-1}) is the maximum adsorption capacity in the Langmuir isotherm model, and K_L (L μmol^{-1}) is the equilibrium constant of the linearized Langmuir isotherm model. $R_L = 1/(1 + K_L C_0)$, derived from K_L, is used to compare the adsorption affinity of the Langmuir isotherms. K_F (μmol$^{1-1/n}$ L$^{1/n}$ g^{-1}) and n (dimensionless) are constants associated with the relative maximum adsorption capacity and adsorption intensity, respectively [24].

The thermodynamic parameters of CAR, PYR, and TEB adsorption were estimated by using Equations (7)–(9) [25].

$$K_d = \frac{Q_e}{C_e}, \tag{7}$$

$$\Delta G° = -RT ln(1000 K_d), \tag{8}$$

$$ln(1000 K_d) = -\frac{\Delta H°}{RT} + \frac{\Delta S°}{R}, \tag{9}$$

where K_d (L g^{-1}) is the partition coefficient; $\Delta G°$ in (kJ mol^{-1}), $\Delta H°$ in (kJ mol^{-1}), and $\Delta S°$ (J mol^{-1}·K) are the Gibbs free energy, enthalpy, and entropy, respectively. R (J mol^{-1}·K) and T (K) are the ideal gas constant (8.314 J mol^{-1}·K) and the absolute temperature of the sample solutions. $\Delta H°$ and $\Delta S°$ were calculated as the slope and intercept in the linear graph of $ln(K_d)$ and $1/T$, respectively.

3. Results and Discussion

3.1. Physicochemical Properties of PSB and PSB$_{OX-A}$

The physicochemical properties (e.g., bulk element and ash contents, the atomic molar ratio, specific surface area, total pore volume, average pore size, and BET isotherms) associated with the adsorption capacity of PSB and PSB$_{OX-A}$ are presented in Figure 1 and Table 2. The bulk element and ash contents of PSB (C = 86.6%, H = 1.6%, O = 3.7%, N = 1.7%, S = 0.1%, and ash = 6.3%) and PSB$_{OX-A}$ (C = 82.1%, H = 1.1%, O = 4.9%, N = 1.3%, S = 0.2%, and ash = 10.5%) have revealed considerable differences due to the successive KMnO$_4$ and KOH modification processes. Furthermore, PSB$_{OX-A}$ presented lower atomic molar ratios of H/C (0.16) than that of PSB (0.23), but the sum of O/C and N/C values for PSB$_{OX-A}$ (0.05) were similar to those of PSB (0.05). These findings indicate that PSB$_{OX-A}$ has a higher aromaticity (H/C value: PSB > PSB$_{OX-A}$) than PSB [26]. Additionally, PSB$_{OX-A}$ had a higher specific surface area and total pore volume than that of PSB, but the average pore size of PSB$_{OX-A}$ was smaller than that of PSB. The specific surface area (1977.6 m^2 g^{-1}) and total pore volume (0.12 cm^3 g^{-1}) of PSB$_{OX-A}$ were significantly greater than those of PSB (specific surface area = 93.9 m^2 g^{-1} and total pore volume = 0.04 cm^3 g^{-1}), given that the porous structures were changed by the successive chemical modification using KMnO$_4$ and KOH [11]. However, the average pore size of PSB$_{OX-A}$ (3.4 nm) was not significantly different from that of PSB (3.8 nm). Therefore, the CAR, PYR, and TEB adsorption capacities of PSB$_{OX-A}$ were expected to be enhanced compared with those of PSB.
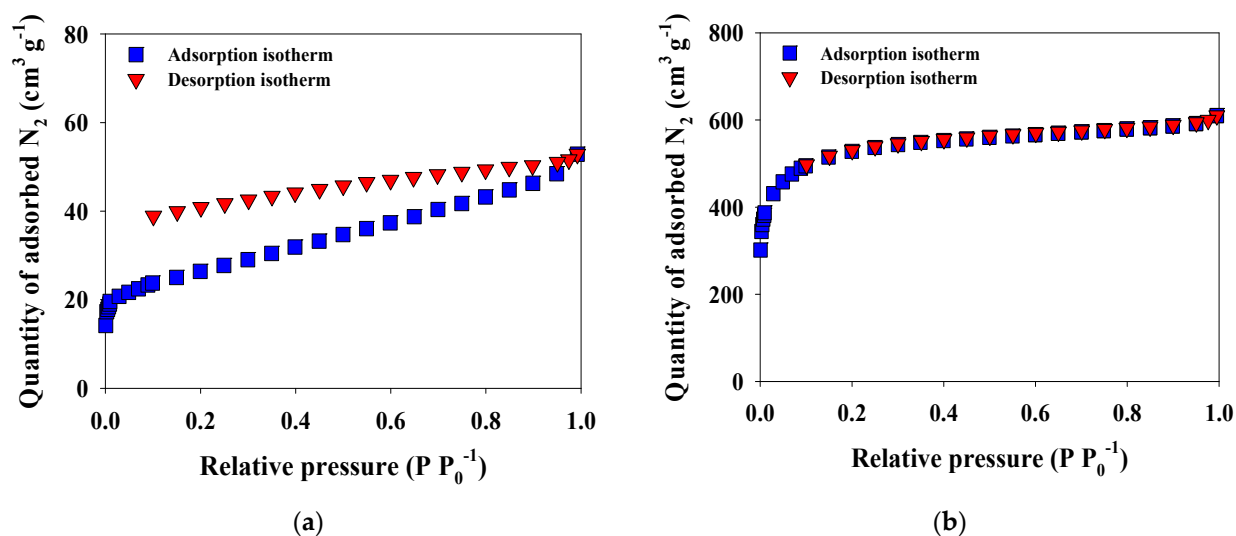
Figure 1. N_2 adsorption-desorption isotherm curves of the (**a**) peanut shell biochar (PSB) and (**b**) $KMnO_4$ and KOH modified PSB (PSB_{OX-A}).

**Table 2.** Physicochemical characteristics of PSB and PSB_{OX-A}.

	Properties	PSB	PSB_{OX-A}
Bulk elemental constitution (%)	C	86.6	82.1
	H	1.6	1.1
	O	3.7	4.9
	N	1.7	1.3
	S	0.1	0.2
	Ash	6.3	10.5
Atomic ratio	H/C	0.2	0.1
	O/C	0.03	0.04
	N/C	0.02	0.01
Specific surface area ($m^2\ g^{-1}$)		93.9	1977.6
Total pore volume ($cm^3\ g^{-1}$)		0.04	0.12
Average pore size (nm)		3.8	3.4

The SEM images of PSB and PSB_{OX-A} are shown in Figure 2. The surface of PSB is smooth and flat, but PSB_{OX-A} has porous and uneven structures. These results indicate that chemical modification using $KMnO_4$ and KOH might change the surface morphology of the PSB with respect to the adsorption of fungicides [27]. The SEM–EDX results of PSB and PSB_{OX-A} demonstrated the effect of chemical modification with $KMnO_4$ and KOH on the differences in the constituents of PSB and PSB_{OX-A}. The PSB_{OX-A} was composed of C (82.05%), O (17.62%), K (0.19%), and Mn (0.14%). However, PSB only consisted of C (85.58%) and O (14.42%). The presence of K and Mn atoms in PSB_{OX-A} could explain why K and Mn were combined on the surface of PSB during the successive chemical modification using $KMnO_4$ and KOH.
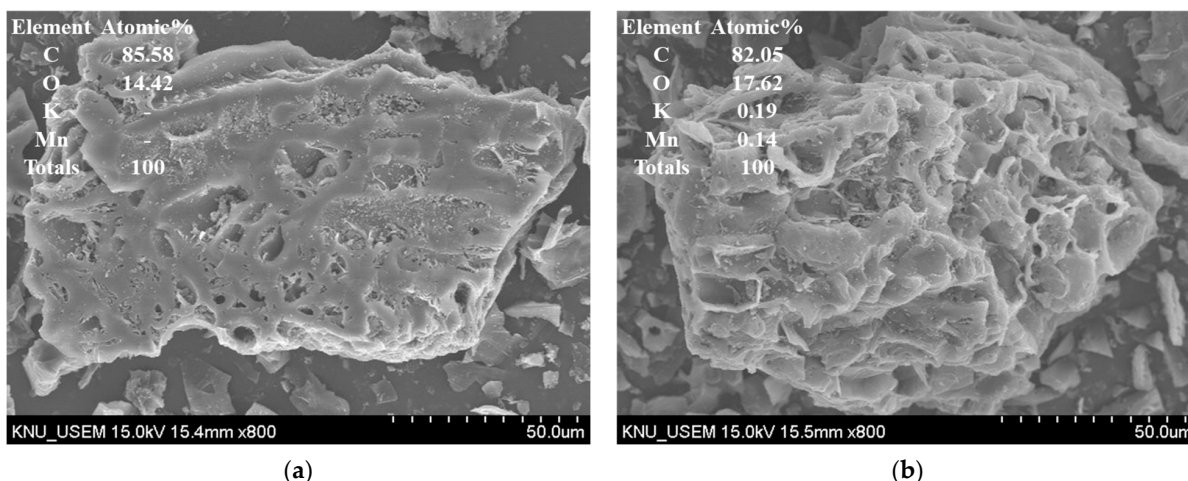
Figure 2. Scanning electron microscopy (SEM) images of (**a**) peanut shell biochar (PSB) and (**b**) $KMnO_4$ and KOH modified PSB (PSB_{OX-A}) (magnification ×800).

Figure 3 shows the FTIR spectra of PSB and PSB_{OX-A}. The IR peak at 3420 cm^{-1} indicates the O-H groups of alcohols [14]. The IR peaks at 1570 and 1180 cm^{-1} could be attributed to the vibrations of the C=C stretching of aromatic groups and the C-O stretching of phenolic and carboxylic groups, respectively [28,29]. The intensities of the IR peaks (i.e., OH alcohol groups, C=C aromatic groups, and C-O phenolic and carboxylic groups) for PSB_{OX-A} were significantly higher than those of PSB. These observations suggest that the differences in the adsorption capacities of PSB and PSB_{OX-A} could influence the adsorption of fungicides because of the successive chemical modifications with $KMnO_4$ and KOH.
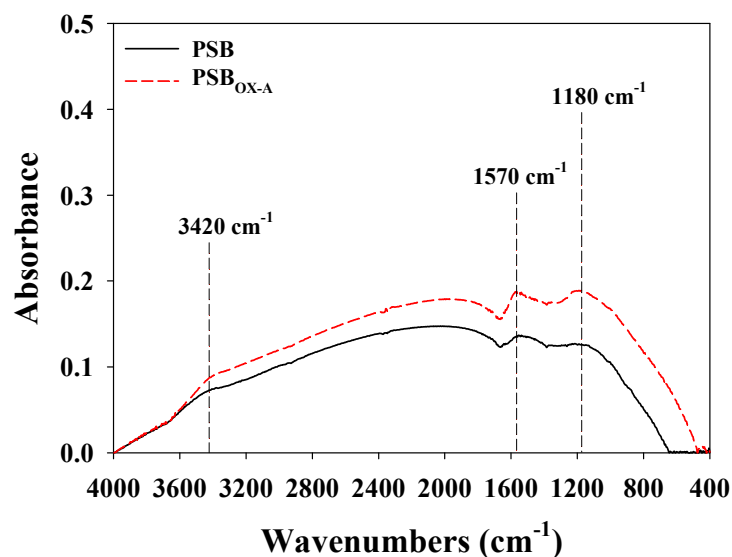
Figure 3. Fourier-transform infrared (FTIR) spectra of PSB and PSB_{OX-A}.

3.2. Effects of Absorbent Dosages

The effects of PSB and PSB_{OX-A} dosages on the removal efficiencies of CAR, PYR, and TEB are shown in Figure 4. The adsorption capacities of CAR, PYR, and TEB using PSB and PSB_{OX-A} continuously decreased, and the removal efficiency of fungicides on PSB and PSB_{OX-A} gradually increased. This is because, when the initial concentrations of CAR, PYR, and TEB are fixed, the adsorption capacity per unit of the adsorbents tends to decline as the amount of PSB and PSB_{OX-A} increases. Similar behavior was previously observed during the removal of the fungicides (e.g., triclosan and triclocarban) using Zr-based magnetic metal–organic frameworks [30]. Based on these experiments on the removal efficiency of

CAR, PYR, and TEB according to the PSB and PSB$_{OX-A}$ dosages, 50 mg L^{-1} was selected as the optimal dosage and applied to the subsequent experiments.
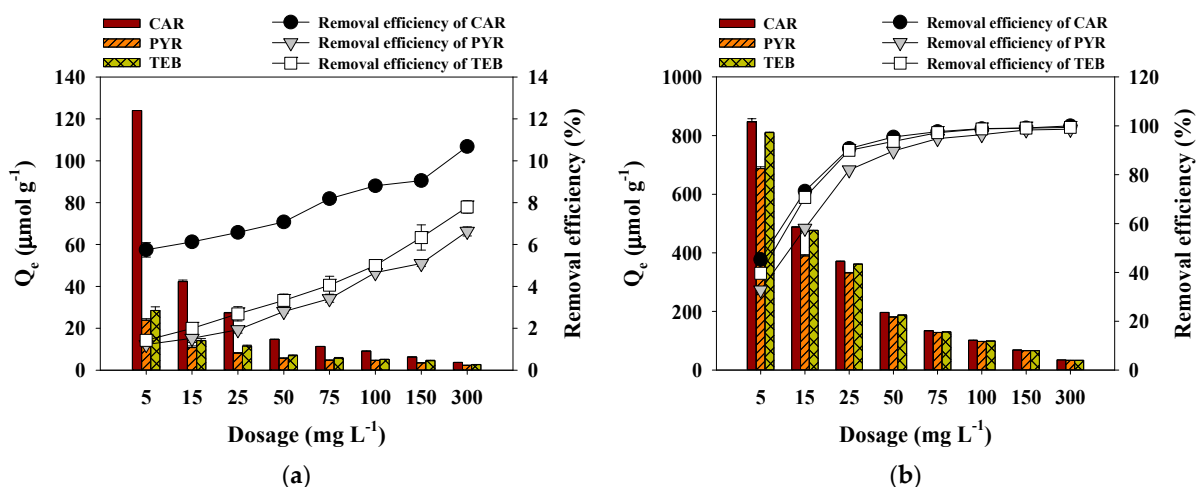
Figure 4. Effects of adsorbent dosages on the removal efficiency of CAR, PYR, and TEB by (**a**) PSB and (**b**) PSB$_{OX-A}$ (agitation speed = 150 rpm; initial concentration of each fungicide = 10 μM; contact time = 24 h; temperature = 25 °C; pH = 7.0).

3.3. Adsorption Kinetics of Fungicides

Figure 5 shows the adsorption kinetics of CAR, PYR, and TEB when using PSB and PSB$_{OX-A}$. The fast adsorption reaction was completed within 4 h for fungicides on the PSB and PSB$_{OX-A}$ surfaces. After 4 h, the removal efficiencies of CAR, PYR, and TEB were increased by PSB and PSB$_{OX-A}$ because the activated binding sites on PSB and PSB$_{OX-A}$ surfaces were saturated [12]. The removal efficiencies of CAR, PYR, and TEB by PSB (removal efficiency of CAR = 7.3 ± 0.04%, removal efficiency of PYR = 3.1 ± 0.04%, and removal efficiency of TEB = 5.8 ± 0.08%) were considerably lower than those of CAR, PYR, and TEB by PSB$_{OX-A}$ (removal efficiency of CAR = 95.1 ± 0.1%, removal efficiency of PYR = 89.9 ± 0.02%, and removal efficiency of TEB = 92.7 ± 0.1%). These observations were attributed to the differences in the physicochemical properties (i.e., specific surface area, total pore volume, and surface functional groups) of PSB and PSB$_{OX-A}$.
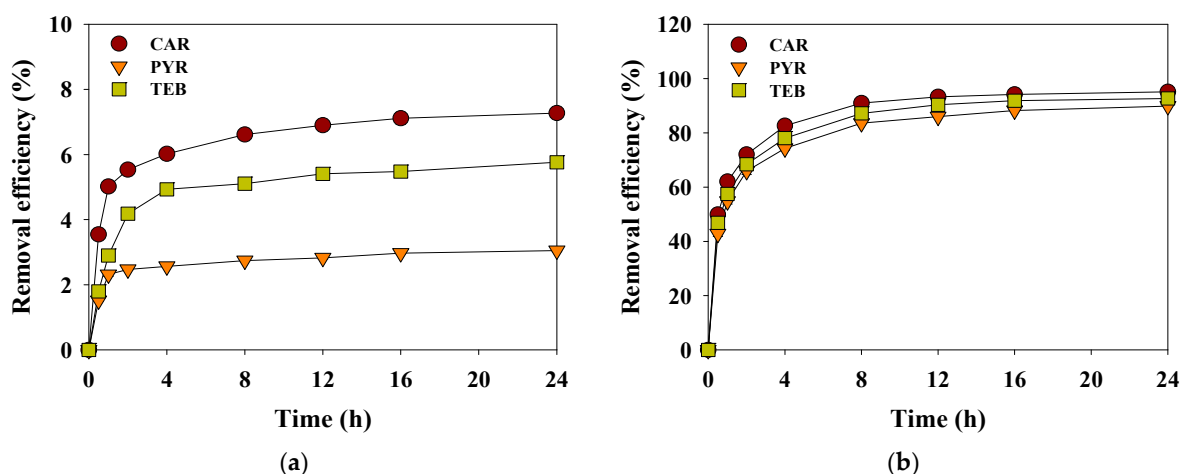
Figure 5. Adsorption kinetics of the selected fungicides using (**a**) PSB and (**b**) PSB$_{OX-A}$ (agitation speed = 150 rpm; absorbent dosage = 50 mg L^{-1}; initial concentration of each fungicide = 10 μM; temperature = 25 °C; pH = 7.0).

Table 3 presents the adsorption kinetics for CAR, PYR, and TEB when using PSB and PSB$_{OX-A}$. The pseudo-second-order model (R^2 = 0.999) might better explain the adsorption of fungicides when using PSB and PSB$_{OX-A}$ than the pseudo-first-order model

(R^2 = 0.882–0.985). The equilibrium adsorption capacities of the fungicides ($Q_{e,exp}$) on those of PSB ($Q_{e,exp}$ of the PSB_{OX-A} = 179.7–196.9 µmol g^{-1}) were much greater than those of PSB ($Q_{e,exp}$ of the PSB = 6.1–15.1 µmol g^{-1}). Furthermore, the $Q_{e,exp}$ values of CAR, PYR, and TEB toward the PSB and PSB_{OX-A} demonstrate similar trends as those of the theoretical adsorption capacities ($Q_{e, cal}$) calculated by the pseudo-second-order model ($Q_{e, cal}$ of the PSB = 6.7–15.4 µmol g^{-1}, $Q_{e, cal}$ of the PSB_{OX-A} = 184.9–202.0 µmol g^{-1}). These results suggested that the adsorption of CAR, PYR, and TEB on PSB and PSB_{OX-A} might be chemisorption [31].

Table 3. Kinetic parameters for the adsorptions of the selected fungicides using PSB and PSB_{OX-A} (agitation speed = 150 rpm; contact time = 24 h; absorbent dosage = 50 mg L^{-1}; initial concentration of each fungicide = 10 µM; temperature = 25 °C; pH = 7.0).

Absorbents	Compounds	$Q_{e,exp}$ (µmol g^{-1})	Pseudo-Fist-Order			Pseudo-Second-Order		
			$Q_{e,cal}$ (µmol g^{-1})	k_1 (1 h^{-1})	R^2	$Q_{e,cal}$ (µmol g^{-1})	k_2 (g µmol^{-1}·h)	R^2
PSB	CAR	15.1 ± 0.1	6.1 ± 0.3	0.2 ± 0.04	0.976	15.4 ± 0.1	0.09 ± 0.01	0.999
	PYR	6.1 ± 0.1	2.1 ± 0.3	0.1 ± 0.02	0.915	6.7 ± 0.05	0.08 ± 0.01	0.999
	TEB	11.6 ± 0.2	5.4 ± 0.6	0.1 ± 0.03	0.882	10.1 ± 0.1	0.2 ± 0.005	0.999
PSB_{OX-A}	CAR	196.9 ± 0.2	81.9 ± 1.1	0.3 ± 0.03	0.983	202.0 ± 0.07	0.008 ± 0.004	0.999
	PYR	179.7 ± 0.06	81.4 ± 1.3	0.2 ± 0.02	0.982	184.9 ± 1.0	0.007 ± 0.003	0.999
	TEB	186.2 ± 0.2	88.3 ± 2.2	0.2 ± 0.05	0.985	192.0 ± 1.6	0.007 ± 0.002	0.999

3.4. Adsorption Isotherms of Fungicides

The adsorption of CAR, PYR, and TEB by PSB and PSB_{OX-A} were examined by using the Langmuir and Freundlich isotherm models (Figure 6 and Table 4). The adsorption behaviors of CAR, PYR, and TEB with respect to PSB and PSB_{OX-A} are better explained by the Langmuir isotherm model (R^2 = 0.996–0.999) than the Freundlich isotherm model (R^2 = 0.764–0.995). This indicated that monolayer adsorption played a key role in removing the fungicides from the homogeneous surfaces of PSB and PSB_{OX-A} [32]. The adsorption affinities of CAR, PYR, and TEB to PSB and PSB_{OX-A} were evaluated by using the R_L values. The R_L values, namely (i) $R_L > 1$: unfavorable, (ii) $R_L = 1$: linear, (iii) $0 < R_L < 1$: favorable, and (iv) $R_L = 0$: irreversible, of the Langmuir isotherm model were used to identify the maximum adsorption capacities of CAR, PYR, and TEB by using PSB and PSB_{OX-A} [33]. The R_L values of PSB and PSB_{OX-A} were estimated to be favorable (R_L = 0.08–0.8).
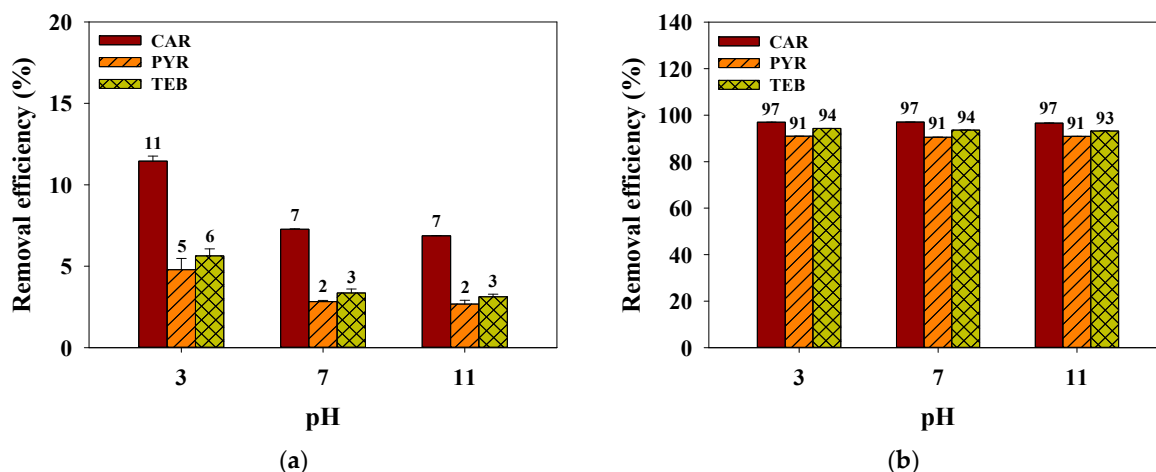

(a)

(b)
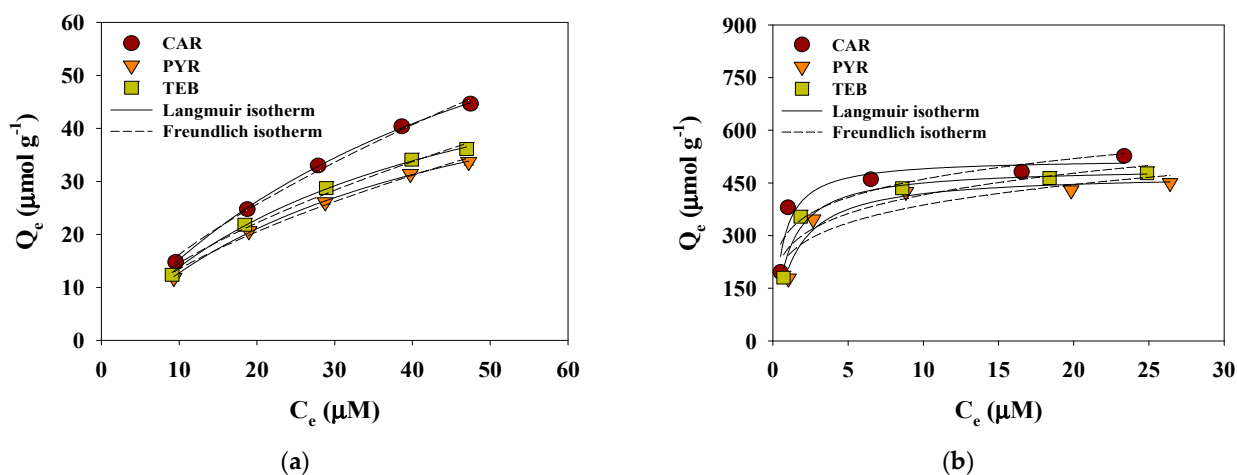
Figure 6. Adsorption isotherms of fungicides on (**a**) PSB and (**b**) PSB_{OX-A} (agitation speed = 150 rpm; contact time = 24 h; absorbent dosage = 50 mg L^{-1}; initial concentration of each fungicide = 10 µM; temperature = 25 °C; pH = 7.0).

Table 4. Isotherm parameters for the adsorptions of fungicides using PSB and PSB$_{OX-A}$ (agitation speed = 150 rpm; contact time = 24 h; absorbent dosage = 50 mg L^{-1}; initial concentration of each fungicide = 10 μM; temperature = 25 °C; pH = 7.0).

Absorbents	Compounds	Langmuir			Freundlich		
		Q_{max} (μmol g^{-1})	K_L (L μmol^{-1})	R^2	n	K_F (μmol$^{1-(1/n)}$ L$^{1/n}$ g^{-1})	R^2
PSB	CAR	92.6 ± 1.3	0.02 ± 0.004	0.999	1.4 ± 0.03	3.1 ± 0.03	0.995
	PYR	61.7 ± 2.2	0.03 ± 0.001	0.998	1.5 ± 0.04	2.9 ± 0.01	0.990
	TEB	66.7 ± 0.5	0.03 ± 0.002	0.996	1.5 ± 0.02	3.0 ± 0.05	0.988
PSB$_{OX-A}$	CAR	531.2 ± 1.9	1.2 ± 0.1	0.997	4.9 ± 0.07	288.9 ± 0.7	0.764
	PYR	467.7 ± 1.2	0.8 ± 0.05	0.999	3.9 ± 0.03	214.9 ± 0.8	0.800
	TEB	495.1 ± 2.5	0.9 ± 0.3	0.999	4.1 ± 0.04	239.1 ± 0.6	0.826

3.5. Effects of pH on Adsorption of Fungicides

Figure 7 depicts the adsorption behaviors of CAR, PYR, and TEB for PSB and PSB$_{OX-A}$ at three different pH values (pH = 3, 7, and 11). The removal efficiencies of CAR (11.5% → 6.9%), PYR (4.8% → 2.7%), and TEB (5.6% → 3.1%) by the PSB were negative affected by the increase of pH values. However, the removal efficiencies of CAR (97.0% → 96.6%) and PYR (91.0% → 90.6%) by the PSB$_{OX-A}$ were not significantly different under the different pH values. The change in pH values strongly influenced the removal efficiency of TEB (94.3% → 93.2%) by the PSB$_{OX-A}$ due to the lower pKa value of TEB (pK$_a$ = 2.01) compared with the CAR (pK$_a$ = 4.28) and PYR (pK$_a$ = 3.44). Moreover, the deprotonated fungicides could promote the electrostatic repulsive interaction between the fungicides and the PSB under the pH value was higher than their pK$_a$ values [12]. These observations could explain that the electrostatic interactions between fungicides and absorbents under the different pH values played a key role in the adsorptions of the CAR, PYR, and TEB using the PSB and PSB$_{OX-A}$.
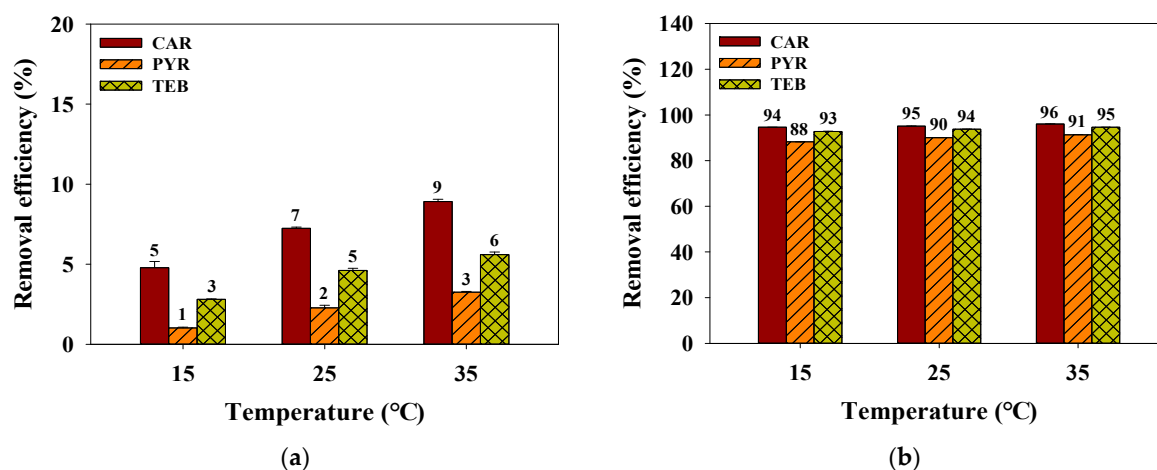

Figure 7. The effects of the pH on the adsorption of fungicides by (**a**) the PSB and (**b**) PSB$_{OX-A}$ (agitation speed = 150 rpm; contact time = 24 h; absorbent dosage = 50 mg L^{-1}; initial concentration of each fungicide = 10 μM; temperature = 25 °C).

3.6. Effects of Temperature and Thermodynamic Studies

The effects of temperature (15–35 °C) on the adsorption of fungicides using PSB and PSB$_{OX-A}$ are illustrated in Figure 8. The removal efficiencies of fungicides using PSB (15 °C: CAR = 4.8 ± 0.4%, PYR = 1.0 ± 0.04%, and TEB = 2.8 ± 0.03%; 25 °C: CAR = 7.2 ± 0.1%, PYR = 2.3 ± 0.2%, and TEB = 4.6 ± 0.1%; 35 °C: CAR = 8.9 ± 0.1%, PYR = 3.3 ± 0.04%, and TEB = 5.6 ± 0.2%) and PSB$_{OX-A}$ (15 °C: CAR = 94.3 ± 0.01%, PYR = 88.2 ± 0.03%, and TEB = 92.8 ± 0.1%; 25 °C: CAR = 94.8 ± 0.02%, PYR = 90.0 ± 0.1%, and TEB = 93.8 ± 0.02%; 35 °C: CAR = 95.8 ± 0.1%, PYR = 91.3 ± 0.1%, and TEB = 94.7 ± 0.01%) increased with

temperature. A similar result was observed for the removal of herbicides by ground coffee residue biochars [14]. Moreover, the adsorption behaviors of CAR, PYR, and TEB using PSB and PSB_{OX-A} showed the same trends (CAR > TEB > PYR) under different temperature conditions. Table 5 shows the results of the thermodynamic parameters ($\Delta G°$, $\Delta H°$, and $\Delta S°$) for CAR, PYR, and TEB adsorption by PSB and PSB_{OX-A} in relation to the absolute temperatures (288–308 K). The $\Delta G° < 0$ values indicated that the adsorption process was spontaneous. The $\Delta H° > 0$ values designated that the adsorption reaction of CAR, PYR, and TEB on PSB and PSB_{OX-A} was endothermic [30]. Low $\Delta H°$ values (<40 kJ mol^{-1}) might be attributed to the physical adsorption [34]. Furthermore, $\Delta S° > 0$ values showed conducive to adsorption stability due to irreversible adsorption [35].

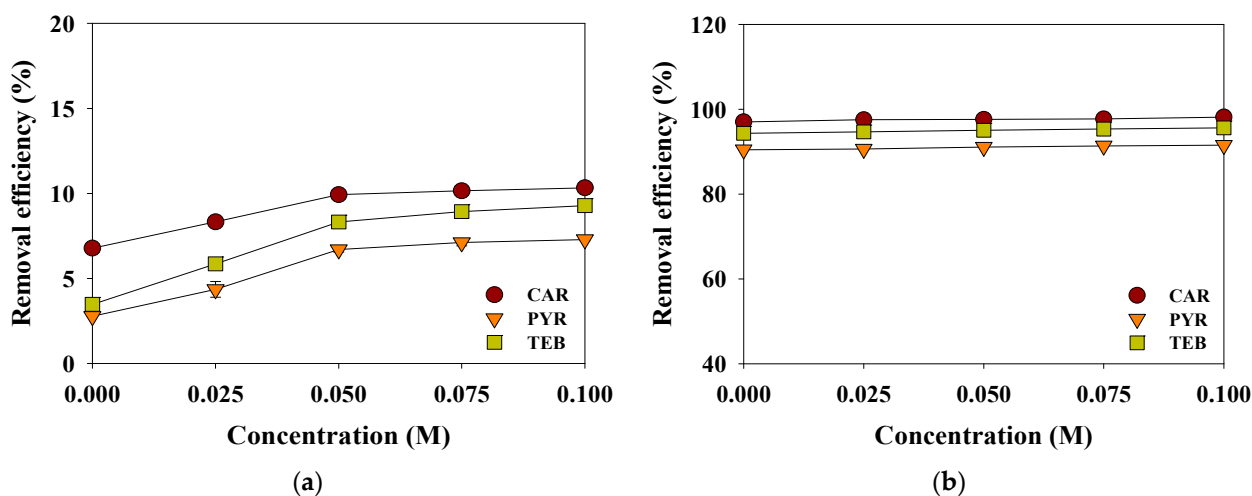**Figure 8.** Effects of temperature on the adsorption of fungicides by (**a**) the PSB and (**b**) PSB_{OX-A} (agitation speed = 150 rpm; contact time = 24 h; absorbent dosage = 50 mg L^{-1}; initial concentration of each fungicide = 10 μM; pH = 7.0).

Table 5. Thermodynamic parameters of fungicides adsorption onto PSB and PSB_{OX-A} (agitation speed = 150 rpm; contact time = 24 h; absorbent dosage = 50 mg L^{-1}; initial concentration of each fungicide = 10 μM; pH = 7.0).

| Adsorbents	Fungicides	Temperature (K)	Thermodynamic Parameters		
			$\Delta G°$ (kJ mol^{-1})	$\Delta H°$ (kJ mol^{-1})	$\Delta S°$ (J mol^{-1} K)
PSB	CAR	288	−16.6 ± 0.4	0.003 ± 0.04	0.048 ± 0.003
		298	−18.3 ± 0.1		
		308	−19.5 ± 0.1		
	PYR	288	−12.8 ± 0.1	0.002 ± 0.0003	0.037 ± 0.001
		298	−15.2 ± 0.2		
		308	−16.7 ± 0.1		
	TEB	288	−15.2 ± 0.1	0.002 ± 0.0004	0.045 ± 0.005
		298	−17.0 ± 0.2		
		308	−18.1 ± 0.2		
PSB_{OX-A}	CAR	288	−31.9 ± 0.1	0.003 ± 0.0005	0.063 ± 0.002
		298	−33.5 ± 0.2		
		308	−35.8 ± 0.3		
	PYR	288	−28.7 ± 0.3	0.005 ± 0.0007	0.090 ± 0.011
		298	−30.1 ± 0.9		
		308	−31.6 ± 0.2		
	TEB	288	−30.0 ± 0.9	0.005 ± 0.0006	0.096 ± 0.013
		298	−31.5 ± 0.2		
		308	−33.0 ± 0.1		

3.7. Effects of NaCl and HA on Adsorption of Fungicides

The effects of ionic strength (NaCl = 0–0.1 M) on the adsorption of CAR, PYR, and TEB by PSB and PSB$_{OX-A}$ are compared in Figure 9. The removal efficiencies of CAR, PYR, and TEB using PSB and PSB$_{OX-A}$ were progressively improved with increasing ionic strengths (PSB: removal efficiency of CAR = 6.8 ± 0.07% → 10.3 ± 0.2%, removal efficiency of PYR = 2.8 ± 0.03% → 7.3 ± 0.08%, removal efficiency of TEB = 3.5 ± 0.1% → 9.3 ± 0.05%; PSB$_{OX-A}$: removal efficiency of CAR = 97.1 ± 0.02% → 98.2 ± 0.01%, removal efficiency of PYR = 90.5 ± 0.01% → 91.6 ± 0.01%, removal efficiency of TEB = 94.3 ± 0.02% → 95.6 ± 0.02%). These findings reveal that reduced solubility of fungicides with increasing concentrations of NaCl can support the adsorption capacity of PSB and PSB$_{OX-A}$ under different ionic strength conditions (salting-out effect) [36,37].

Figure 9. Effects of NaCl concentration on the adsorption of fungicides by (**a**) PSB and (**b**) PSB$_{OX-A}$ (agitation speed = 150 rpm; contact time = 24 h; absorbent dosage = 50 mg L^{-1}; initial concentration of each fungicide = 10 μM; temperature = 25 °C; pH = 7.0).

The effects of HA on the adsorption of CAR, PYR, and TEB for PSB and PSB$_{OX-A}$ are presented in Figure 10. HA, macromolecular compounds with many reactive functional groups, might scavenge the binding sites generated on PSB and PSB$_{OX-A}$. Thus, HA used in the batch experiments could affect the adsorption affinity of fungicides with adsorbents [38]. The removal efficiencies of CAR, PYR, and TEB by PSB are similar to the existence of HA (removal efficiency without HA: CAR = 7.1 ± 0.07%, PYR = 2.8 ± 0.09%, and TEB = 4.3 ± 0.3%; removal efficiency with HA: CAR = 6.8 ± 0.3%, PYR = 2.4 ± 0.2%, and TEB = 2.8 ± 0.1%). The removal efficiencies of CAR, PYR, and TEB using PSB$_{OX-A}$ are not significantly affected by the presence of HA (removal efficiency without HA: CAR = 95.2 ± 0.02%, PYR = 89.7 ± 0.07%, and TEB = 93.7 ± 0.02%; removal efficiency with HA: CAR = 93.8 ± 0.3%, PYR = 88.9 ± 0.3%, and TEB = 93.3 ± 0.07%). These observations suggested that the adsorption behavior of CAR, PYR, and TEB by PSB and PSB$_{OX-A}$ were outcompeted by HA adsorption [12].
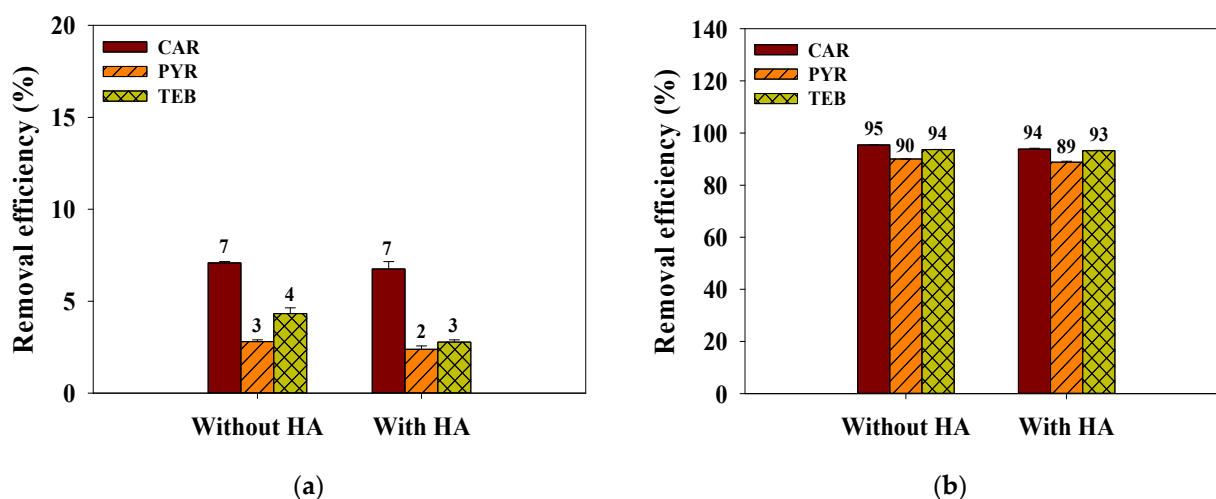
Figure 10. Effects of humic acids (HA) on the adsorption of the fungicides by (**a**) PSB and (**b**) PSB$_{OX-A}$ (the concentration of HA = 5 mg L^{-1}, agitation speed = 150 rpm; contact time = 24 h; absorbent dosage = 50 mg L^{-1}; initial concentration of each fungicide = 10 μM; temperature = 25 °C; pH = 7.0).

4. Conclusions

This study examined the effects of successive KMnO$_4$ and KOH modifications on the physicochemical properties of PSB associated with the adsorption behaviors of CAR, PYR, and TEB. Compared to PSB, PSB$_{OX-A}$ presented a higher specific surface area (1977.6 m^2 g^{-1}) and total pore volume (0.12 cm^3 g^{-1}). The PSB and PSB$_{OX-A}$ were well fitted with the pseudo-second-order kinetic (R^2 = 0.999), and the equilibrium adsorption capacities of CAR, PYR, and TEB on PSB$_{OX-A}$ ($Q_{e,exp}$ = 179.7–196.9 μmol g^{-1}) were greater than those of PSB ($Q_{e,exp}$ = 6.1–15.1 μmol g^{-1}). These findings indicate that chemisorption plays a crucial role in the adsorption of CAR, PYR, and TEB. Moreover, the Langmuir isotherms predominantly governed the removal of fungicides from the homogeneous surfaces of PSB and PSB$_{OX-A}$ (monolayer adsorption, R^2 = 0.996–0.999). The removal efficiencies of CAR, PYR, and TEB using PSB and PSB$_{OX-A}$ gradually increased with increasing temperature and NaCl concentration. Although HA could interfere with CAR, PYR, and TEB adsorptions by PSB and PSB$_{OX-A}$, the removal efficiencies of fungicides by PSB$_{OX-A}$ (88.9–93.8%) were higher when compared to PSB (2.4–6.8%). These results suggest that successive KMnO$_4$ and KOH modification may be a promising option in improving the adsorption capacities of PSB for removing CAR, PYR, and TEB from a real-scale water treatment plant. Future studies need to provide the information for optimum reuse conditions to regenerate the peanut shell biochars with continuous adsorption ability.

Author Contributions: Conceptualization, Y.-G.L.; methodology, Y.-G.L.; validation, Y.-G.L.; formal analysis, S.K. and C.S.; investigation, J.S. and J.K.; data curation, Y.-G.L.; writing—original draft preparation, Y.-G.L.; writing—review and editing, C.-H.L. and K.C.; supervision, K.C.; funding acquisition, G.-Y.K. All authors have read and agreed to the published version of the manuscript.

Conflicts of Interest: The authors declare no conflict of interest.

References

1. Gupta, P.K. Toxicity of fungicides. In *Veterinary Toxicology*, 3rd ed.; Academic Press: Cambridge, MA, USA, 2018; pp. 569–580.
2. Wang, T.; Zhang, Z.; Zhang, H.; Zhong, X.; Liu, Y.; Liao, S.; Yue, X.; Zhou, G. Sorption of carbendazim on activated carbons derived from rape straw and its mechanism. *RSC Adv.* **2019**, *9*, 41745–41754. [CrossRef]
3. Merel, S.; Benzing, S.; Gleiser, C.; di Napoli-Davis, G.; Zwiener, C. Occurrence and overlooked sources of the biocide carbendazim in wastewater and surface water. *Environ. Pollut.* **2018**, *239*, 512–521. [CrossRef]

4. Meng, Y.; Zhong, K.; Xiao, J.; Huang, Y.; Wei, Y.; Tang, L.; Chen, S.; Wu, J.; Ma, J.; Cao, Z.; et al. Exposure to pyrimethanil induces developmental toxicity and cardiotoxicity in zebrafish. *Chemosphere* **2020**, *255*, 126889. [CrossRef] [PubMed]

5. Li, S.; Wu, Q.; Sun, Q.; Coffin, S.; Gui, W.; Zhu, G. Parental exposure to tebuconazole causes thyroid endocrine disruption in zebrafish and developmental toxicity in offspring. *Aquat. Toxicol.* **2019**, *211*, 116–123. [CrossRef]

6. Hgeig, A.; Novaković, M.; Mihajlović, I. Sorption of carbendazim and linuron from aqueous solutions with activated carbon produced from spent coffee grounds: Equilibrium, kinetic and thermodynamic approach. *J. Environ. Sci. Health Part B* **2019**, *54*, 226–236. [CrossRef] [PubMed]

7. Ma, X.; Ouyang, F. Adsorption properties of biomass-based activated carbon prepared with spent coffee grounds and pomelo skin by phosphoric acid activation. *Appl. Surf. Sci.* **2013**, *268*, 566–570. [CrossRef]

8. Wang, Z.; Zhang, J.; Hu, B.; Yu, J.; Wang, J.; Guo, X. Graphene/Fe_3O_4 nanocomposite for effective removal of ten triazole fungicides from water solution: Tebuconazole as an example for investigation of the adsorption mechanism by experimental and molecular docking study. *J. Taiwan Inst. Chem. Eng.* **2019**, *95*, 635–642. [CrossRef]

9. Chen, F.; Song, Z.; Nie, J.; Yu, G.; Li, Z.; Lee, M. Ionic liquid-based carbon nanotube coated magnetic nanoparticles as adsorbent for the magnetic solid phase extraction of triazole fungicides from environmental water. *RSC Adv.* **2016**, *6*, 81877–81885. [CrossRef]

10. Yuan, M.; Tong, S.; Zhao, S.; Jia, C.Q. Adsorption of polycyclic aromatic hydrocarbons from water using petroleum coke-derived porous carbon. *J. Hazard. Mater.* **2010**, *181*, 1115–1120. [CrossRef] [PubMed]

11. An, Q.; Jiang, Y.-Q.; Nan, H.-Y.; Yu, Y.; Jiang, J.-N. Unraveling sorption of nickel from aqueous solution by KMnO4 and KOH-modified peanut shell biochar: Implicit mechanism. *Chemosphere* **2019**, *214*, 846–854. [CrossRef]

12. Shin, J.; Lee, Y.-G.; Lee, S.-H.; Kim, S.; Ochir, D.; Park, Y.; Kim, J.; Chon, K. Single and competitive adsorptions of micropollutants using pristine and alkali-modified biochars from spent coffee grounds. *J. Hazard. Mater.* **2020**, *400*, 123102. [CrossRef]

13. Suo, F.; You, X.; Ma, Y.; Li, Y. Rapid removal of triazine pesticides by P doped biochar and the adsorption mechanism. *Chemosphere* **2019**, *235*, 918–925. [CrossRef]

14. Lee, Y.-G.; Shin, J.; Kwak, J.; Kim, S.; Son, C.; Cho, K.H.; Chon, K. Effects of NaOH Activation on Adsorptive Removal of Herbicides by Biochars Prepared from Ground Coffee Residues. *Energies* **2021**, *14*, 1297. [CrossRef]

15. Zhou, Y.; Liu, X.; Xiang, Y.; Wang, P.; Zhang, J.; Zhang, F.; Wei, J.; Luo, L.; Lei, M.; Tang, L. Modification of biochar derived from sawdust and its application in removal of tetracycline and copper from aqueous solution: Adsorption mechanism and modelling. *Bioresour. Technol.* **2017**, *245*, 266–273. [CrossRef]

16. Wilson, K.; Yang, H.; Seo, C.W.; Marshall, W.E. Select metal adsorption by activated carbon made from peanut shells. *Bioresour. Technol.* **2006**, *97*, 2266–2270. [CrossRef]

17. Allen, S.J.; Gan, Q.; Matthews, R.; Johnson, P.A. Mass transfer processes in the adsorption of basic dyes by peanut hulls. *Ind. Eng. Chem. Res.* **2005**, *44*, 1942–1949. [CrossRef]

18. Johns, M.M.; Marshall, W.E.; Toles, C.A. Agricultural by-products as granular activated carbons for adsorbing dissolved metals and organics. *J. Chem. Technol. Biotechnol.* **1998**, *71*, 131–140. [CrossRef]

19. McConvey, I.F.; Woods, D.; Lewis, M.; Gan, Q.; Nancarrow, P. The Importance of Acetonitrile in the Pharmaceutical Industry and Opportunities for its Recovery from Waste. *Org. Process Res. Dev.* **2012**, *16*, 612–624. [CrossRef]

20. Fu, Y.; Shen, Y.; Zhang, Z.; Ge, X.; Chen, M. Activated bio-chars derived from rice husk via one- and two-step KOH-catalyzed pyrolysis for phenol adsorption. *Sci. Total Environ.* **2019**, *646*, 1567–1577. [CrossRef]

21. Liu, R.; Liu, G.; Yousaf, B.; Abbas, Q. Operating conditions-induced changes in product yield and characteristics during thermal-conversion of peanut shell to biochar in relation to economic analysis. *J. Clean. Prod.* **2018**, *193*, 479–490. [CrossRef]

22. Bhainsa, K.C.; D'souza, S. Removal of copper ions by the filamentous fungus, Rhizopus oryzae from aqueous solution. *Bioresour. Technol.* **2008**, *99*, 3829–3835. [CrossRef]

23. Gorgievski, M.; Božić, D.; Stanković, V.; Štrbac, N.; Šerbula, S. Kinetics, equilibrium and mechanism of Cu^{2+}, Ni^{2+} and Zn^{2+} ions biosorption using wheat straw. *Ecol. Eng.* **2013**, *58*, 113–122. [CrossRef]

24. Hayati, B.; Mahmoodi, N.M. Modification of activated carbon by the alkaline treatment to remove the dyes from wastewater: Mechanism, isotherm and kinetic. *Desalination Water Treat.* **2012**, *47*, 322–333. [CrossRef]

25. Li, R.; Wang, Z.; Guo, J.; Li, Y.; Zhang, H.; Zhu, J.; Xie, X. Enhanced adsorption of ciprofloxacin by KOH modified biochar derived from potato stems and leaves. *Water Sci. Technol.* **2018**, *77*, 1127–1136. [CrossRef] [PubMed]

26. Zhang, J.; Ma, X.; Yuan, L.; Zhou, D. Comparison of adsorption behavior studies of Cd^{2+} by vermicompost biochar and KMnO₄-modified vermicompost biochar. *J. Environ. Manag.* **2020**, *256*, 109959. [CrossRef] [PubMed]

27. Bian, S.; Xu, S.; Yin, Z.; Liu, S.; Li, J.; Xu, S.; Zhang, Y. An Efficient Strategy for Enhancing the Adsorption Capabilities of Biochar via Sequential KMnO4-Promoted Oxidative Pyrolysis and H_2O_2 Oxidation. *Sustainability* **2021**, *13*, 2641. [CrossRef]

28. Huff, M.D.; Kumar, S.; Lee, J.W. Comparative analysis of pinewood, peanut shell, and bamboo biomass derived biochars produced via hydrothermal conversion and pyrolysis. *J. Environ. Manag.* **2014**, *146*, 303–308. [CrossRef]

29. Acemioğlu, B. Removal of a reactive dye using NaOH-activated biochar prepared from peanut shell by pyrolysis process. *Int. J. Coal Prep. Util.* **2019**, 1–23. [CrossRef]

30. Ahmad, M.; Lee, S.S.; Dou, X.; Mohan, D.; Sung, J.-K.; Yang, J.E.; Ok, Y.S. Effects of pyrolysis temperature on soybean stover- and peanut shell-derived biochar properties and TCE adsorption in water. *Bioresour. Technol.* **2012**, *118*, 536–544. [CrossRef]

31. Ma, J.; Li, S.; Wu, G.; Arabi, M.; Tan, F.; Guan, Y.; Li, J.; Chen, L. Preparation of magnetic metal-organic frameworks with high binding capacity for removal of two fungicides from aqueous environments. *J. Ind. Eng. Chem.* **2020**, *90*, 178–189. [CrossRef]

32. Kim, E.; Jung, C.; Han, J.; Her, N.; Park, C.M.; Jang, M.; Son, A.; Yoon, Y. Sorptive removal of selected emerging contaminants using biochar in aqueous solution. *J. Ind. Eng. Chem.* **2016**, *36*, 364–371. [CrossRef]

33. Shin, J.; Lee, Y.-G.; Kwak, J.; Kim, S.; Lee, S.-H.; Park, Y.; Lee, S.-D.; Chon, K. Adsorption of radioactive strontium by pristine and magnetic biochars derived from spent coffee grounds. *J. Environ. Chem. Eng.* **2021**, *9*, 105119. [CrossRef]

34. Fan, S.; Tang, J.; Wang, Y.; Li, H.; Zhang, H.; Tang, J.; Wang, Z.; Li, X. Biochar prepared from co-pyrolysis of municipal sewage sludge and tea waste for the adsorption of methylene blue from aqueous solutions: Kinetics, isotherm, thermodynamic and mechanism. *J. Mol. Liq.* **2016**, *220*, 432–441. [CrossRef]

35. Son, C.; An, W.; Lee, G.; Jeong, I.; Lee, Y.-G.; Chon, K. Adsorption Characteristics of Phosphate Ions by Pristine, $CaCl_2$ and $FeCl_3$-Activated Biochars Originated from Tangerine Peels. *Separations* **2021**, *8*, 32. [CrossRef]

36. Xiao, X.; Sheng, G.D.; Qiu, Y. Improved understanding of tributyltin sorption on natural and biochar-amended sediments. *Environ. Toxicol. Chem.* **2011**, *30*, 2682–2687. [CrossRef]

37. Xiang, Y.; Xu, Z.; Zhou, Y.; Wei, Y.; Long, X.; He, Y.; Zhi, D.; Yang, J.; Luo, L. A sustainable ferromanganese biochar adsorbent for effective levofloxacin removal from aqueous medium. *Chemosphere* **2019**, *237*, 124464. [CrossRef]

38. Cano-Aguilera, I.; Haque, N.; Morrison, G.M.; Aguilera-Alvarado, A.F.; Gutiérrez, M.; Gardea-Torresdey, J.L.; de la Rosa, G. Use of hydride generation-atomic absorption spectrometry to determine the effects of hard ions, iron salts and humic substances on arsenic sorption to sorghum biomass. *Microchem. J.* **2005**, *81*, 57–60. [CrossRef]